

Modelling globular clusters as multi-wavelength emitters

Hambeleleni Davids,^{a,b,*} Christo Venter^b and Michael Backes^{c,b}

^a*Department of Science Foundation, School of Science, University of Namibia,
Private Bag 13301, Windhoek 10005 Namibia*

^b*Centre for Space Research, North-West University, Potchefstroom Campus,
Private Bag X6001, Potchefstroom 2520, South Africa*

^c*University of Namibia, Department of Physics, Chemistry & Material Science,
Windhoek Campus, Private Bag 13301, Windhoek, Namibia*

E-mail: hndiyavala@unam.na, christo.venter@nwu.ac.za, mbackes@unam.na

At present, only a single globular cluster (GC) has plausibly been detected at very high energies (VHEs) by H.E.S.S. The future Cherenkov Telescope Array (CTA) is expected to detect more GCs in this band. We present results from an emission code that assumes millisecond pulsars (MSPs) to be sources of relativistic particles diffusing through GCs that will give broad-band radiation due to their interaction with the cluster magnetic and soft-photon fields. We perform a parameter study to investigate the GC model's behaviour and study the detectability of Galactic GCs for H.E.S.S. and CTA. We also present new *Fermi* LAT data on Terzan 5 and model its broadband spectrum, constraining our model with available multi-wavelength data. We furthermore derive constraints on the embedded population of MSPs' luminosity function. Finally, we note that stacking upper limits by H.E.S.S. on the γ -ray flux of a population of 15 Galactic GCs are very constraining for leptonic emission models. We therefore show that uncertainty in model parameters leads to a large spread in the predicted flux, and there are indeed regions in parameter space for which the stacking upper limits are satisfied.

*** *High Energy Astrophysics in Southern Africa (HEASA2021)* ***

*** *13 - 17 September, 2021* ***

*** *Online* ***

*Speaker

1. Introduction

GCs are gravitationally bound, ancient stellar systems consisting of $10^4 - 10^6$ stars, with ages ranging between 11 and 13 Gyr [1]. There are about 160 known GCs in the Milky Way [2], distributed roughly spherically about the Galactic Centre and lying at an average radius of 12 kpc from it. A large variety of exotic objects populate the dense environment of GCs [3], including black holes, millisecond pulsars (MSPs), white dwarfs and Cataclysmic variables.

GCs are visible from radio [4] to γ -ray energies. Detections include diffuse radio [5] and diffuse X-ray emission [6–8] from 47 Tucanane and Terzan 5, as well as detection of X-ray point sources in some GCs [9]. While pulsars are not readily detectable at optical wavelengths among the stellar emission in the cluster, some of their companions [10, 11] and also types of exotic binaries are detectable. About two dozen GCs have been observed by *Fermi* LAT, which detect photons in the energy range of 20 MeV to 300 GeV [12]. H.E.S.S., which is a ground-based Cherenkov telescope operated in a pointing mode, has plausibly¹ detected only a single Galactic cluster (Terzan 5) at VHEs (> 100 GeV) [13]. Other Cherenkov telescopes could only produce upper limits to GC VHE emission [14–16].

Within the MSP scenario [17], several GC emission components are thought to originate from cumulative magnetospheric and diffuse emission by particles accelerated either within the embedded pulsar magnetospheres or in interstellar/binary shocks. In this paper, we summarize our recent GC modelling efforts [18–22]. First, we conduct a parameter study and also probe the detectability of 16 Galactic GCs for H.E.S.S. and CTA, ranking them according to their predicted TeV flux using a leptonic emission model. Second, we constrain model parameters for individual GCs using γ -ray and X-ray data. Third, we gather more data on Terzan 5 and model its updated broadband spectral energy distribution (SED). We additionally derive constraints on the MSP luminosity function using the diffuse X-ray data and *Chandra* sensitivity. Lastly, we demonstrate that uncertainty in GC model parameters leads to a large spread in the predicted flux, and there are indeed regions in parameter space for which the stringent stacking upper limits by H.E.S.S. on 15 GCs are satisfied.

2. The Models

2.1 The Leptonic Emission Model for GCs

We use a multi-zone, steady-state, spherically symmetric model [17] that calculates the particle transport (1D: radial spatial coordinate) and observed spectrum for GCs. The model predicts the SED from GCs by considering unpulsed synchrotron radiation (SR) as well as inverse Compton (IC) emission, attributing this to the interaction of collective leptonic winds with the ambient magnetic and soft-photon fields [17]. A Fokker-Planck type equation in [23] is solved numerically

$$\frac{\partial n_e}{\partial t} = \vec{\nabla} \cdot (\vec{\kappa} \cdot \vec{\nabla} n_e) - \frac{\partial}{\partial E_e} [\dot{E}_e n_e(E_e, r_s)] + Q(E_e), \quad (1)$$

where n_e is the electron density per energy and volume, which is a function of central GC radius $r_s = |\vec{r}_s|$, E_e the electron energy, $\vec{\kappa}$ is the diffusion tensor, \dot{E}_e the radiation losses, and Q the electron source term. In order to calculate the IC losses \dot{E}_{IC} , we consider blackbody soft-photon

¹The probability for a chance detection in this direction is $\sim 10^{-4}$.

densities due to the cosmic microwave background and photons from stars with a temperature of $T_1 = 4\,500\text{ K}$. For the soft-photon component we use a line-of-sight (LOS) integration [24]. We assume a constant B -field in the case of SR to calculate the SR losses. Two different diffusion coefficients are considered: 1) Bohm diffusion with $\kappa(r_s, E_e) = cE_e/3eB$, where B is the GC B -field, c the speed of light, and e the electron charge; and a diffusion coefficient inspired by Galactic cosmic-ray propagation studies with $\kappa(r_s, E_e) = \kappa_0(E_e/E_0)^\alpha$, where $E_0 = 1\text{ TeV}$ and $\alpha = 0.6$ (see, e.g., [25]). We lastly use a power-law particle injection spectrum $Q(E_e) = Q_0E_e^{-\Gamma}$, with units of $\text{erg}^{-1}\text{s}^{-1}$, between energies $E_{e,\text{min}}$ and $E_{e,\text{max}}$ and slope Γ . This is motivated by the fact that H.E.S.S. detected a power-law spectrum for the VHE source associated with Terzan 5.

2.2 The Pulsar Magnetospheric Emission Model

We also use a pulsar emission model [26] that predicts the broad-band X-ray to VHE γ -ray pulsed spectrum of pulsars. Primaries are injected at the stellar surface; they produce curvature radiation (CR) γ rays that are converted into pairs via magnetic pair creation. The electron-positron pairs lose their momentum perpendicular to the magnetic field to SR near the polar caps and then coast into the outer magnetosphere where they may encounter radio photons that may increase their pitch angles, leading to further emission of SR. The model also includes CR radiation of primary particles accelerated by electron fields in a slot gap geometry. The model assumes a force-free magnetosphere configuration as an improvement over the retarded vacuum dipole.

3. Parameter Study Involving the Leptonic Model

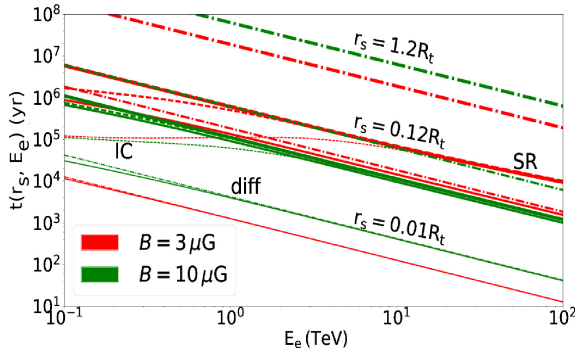


Figure 1: Loss timescales as a function of energy. The solid lines indicate effective timescales, the dashed lines represent (diffuse) radiation losses, and diffusion is shown by dash-dotted lines.

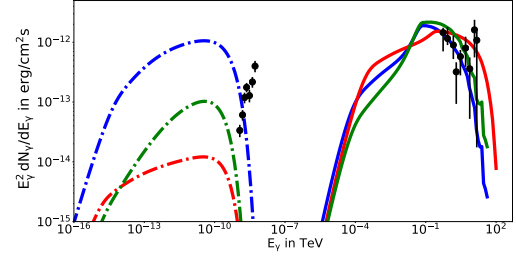


Figure 2: The predicted SED for Terzan 5 indicating the SR (integrated between $55' < r_s < 174'$, the dash-dotted lines) for the inner part of the source and IC (integrated over all r_s , solid lines) for the diffuse emission components for different combinations of parameters, as well as *Chandra* [6] and H.E.S.S. [13] data.

We have performed an extensive parameter study using the leptonic emission model for GCs [20]. As an example, we present the effect of a changing cluster B -field here. **Figure 1** presents the timescales for only the diffuse GC emission. It can be seen that for a lower B -field, the SR timescale is longer (i.e., $t_{\text{SR}} = E_e/\dot{E}_{\text{SR}} \propto E_e^{-1}B^{-2}$). It therefore takes a longer time for particles to lose energy due to SR. Also, the diffusion timescale is relatively shorter in the Bohm limit, and hence particles will escape faster from a particular zone in this case. We also note that IC dominates

SR at low energies whilst SR dominates diffusion at large r_s . An interesting regime change occurs between IC and SR domination around $\lesssim 1$ TeV for these two B -field strengths: for $B = 10 \mu\text{G}$, SR dominates over IC for $E_e \gtrsim \text{TeV}$, while this change occurs around $E_e \gtrsim 10 \text{ TeV}$ for $B = 3 \mu\text{G}$.

4. Ranking of Galactic GCs According to Their Predicted VHE Flux

We applied the GC model to 15 non-detected GCs and to Terzan 5. We assumed Bohm diffusion, $\Gamma = 2.0$, $B = 5 \mu\text{G}$, and $E_{e,\text{max}} = 100 \text{ TeV}$. Our predictions show that H.E.S.S. may detect two more Galactic GCs (i.e., 47 Tucanae and NGC 6388 in addition to Terzan 5 if the GCs are observed for 100h. The flux prediction and the ranking are very sensitive to the choice of parameters. Also, if there are X-ray data that can be treated as an upper limit to the SR spectral component, this may reduce the TeV flux somewhat; however, the available X-ray data on GCs are typically very scarce and unconstraining, and we do not expect this to impact the TeV predictions substantially. The CTA may detect many more GCs than H.E.S.S. since it will be 10 times more sensitive. The top five promising GCs (see Figure 3) for CTA that we found are NGC 6388, 47 Tucanae, Terzan 5, Djorg 2, and Terzan 10.

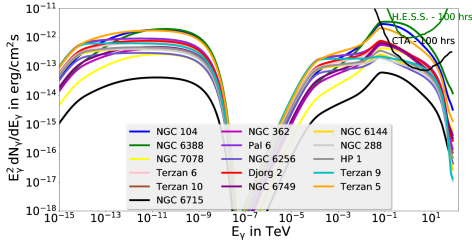


Figure 3: SED showing GCs ranked according to their predicted fluxes. The H.E.S.S. and CTA sensitivities (for 100 hours) are also shown. This is for the diffuse emission components.

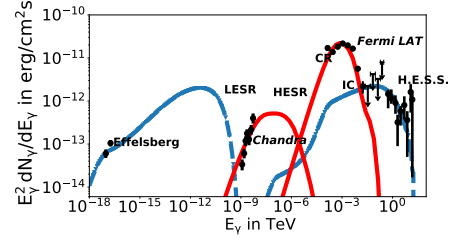


Figure 4: Spectral components for Terzan 5 predicted by the leptonic models of [17] and [26]. We also indicate *Chandra* [6], H.E.S.S. [13], and radio data [“Region 11” as defined by 5].

5. Multi-wavelength Data on Terzan 5

Below, we model the broadband SED of Terzan 5. This object hosts the largest number of MSPs (i.e., 37 MSPs) [27] detected so far and exhibits the highest central stellar density. It is also the only GC that has plausibly been detected at VHE [13].

5.1 Radio Emission

The Very Large Array (VLA) of the National Radio Astronomy Observatory (NRAO) Sky Survey (NVSS) detected the GC Terzan 5 at 21 cm as a single source with a flux of 5 mJy. Effelsberg 11 cm and 21 cm archival data revealed several radio structures in the direction of Terzan 5 [5].

5.2 Estimation of the Optical Background Level

The predicted non-thermal unpulsed low-energy synchrotron radiation (LESR) spectral component invoked to model the radio data extends into the optical band. However, the LESR component

is at low flux level and it will be difficult to detect this component, since there are many stars ($\sim 10^5$) that contribute a high level of blackbody radiation that may swamp any diffuse non-thermal emission SR. We estimate a thermal νF_ν flux of $\sim 1.7 \times 10^{-14} R_{10}^2 N_{\text{ann}} \text{ erg cm}^{-2} \text{ s}^{-1}$ assuming $R_{10} = R/10^{10} \text{ cm}$, $d = 5.9 \text{ kpc}$, and c the speed of light. We find that the predicted blackbody flux is $\sim 10^5$ higher than the estimated LESR flux level of the full GC.

5.3 Diffuse X-ray Emission

Eger et al. [6] discovered the presence of hard and diffuse X-ray emission above the particle background level from Terzan 5. We fit the diffuse X-ray data by invoking a new high-energy synchrotron radiation (HESR) component that may be due to the cumulative pulsed magnetospheric SR from pairs (see Figure 4).

5.4 High-Energy Emission *Fermi* LAT Data Analysis

Terzan 5 is the second γ -ray-emitting GC to be associated with a *Fermi* LAT source after 47 Tucanae. The total number of MSPs in Terzan 5 is $N_{\text{MSP}} = 180_{-90}^{+100}$, estimated using the average MSP spin-down power ($\langle \dot{E} \rangle$ of Galactic MSPs known at the time) and the measured γ -ray flux [28]. We considered seven years of Pass 8 (P8) LAT data and these data are fit with cumulative pulsed magnetospheric CR from primaries and proved to be constraining for the low-energy tail of the unpulsed IC component.

5.5 Very-High-Energy (VHE) Emission: H.E.S.S. Data

H.E.S.S. discovered a VHE γ -ray source HESS J1747–248, located in the direction of Terzan 5. The spectrum of the source is described by a power law with index of $2.5 \pm 0.3_{\text{stat}} \pm 0.2_{\text{sys}}$ [13]. The probability of a chance coincidence between an unrelated VHE γ -ray source and Terzan 5 is low ($\sim 10^{-4}$). Unfortunately, no new observations have been carried out on this source since its discovery [13].

6. Initial Constraining of Model Parameters of Particular GCs

We constrained cluster parameters for three GCs (i.e., Terzan 5, 47 Tucanae, and NGC 6388) using diffuse X-ray and VHE γ -ray observations. As an example, we present the results for Terzan 5. The The diffuse γ -ray [13] and X-ray [6] data plus model fit are shown in Figure 2. Unfortunately, the GC model cannot reproduce the flat slope of the X-ray data. We therefore postulate a new radiation component (the HESR component) to explain these data. We treat the X-ray data as upper limits to the LESR component. We try to find sample parameters so that the predicted SR component is not in conflict with the X-ray “upper limits”, while at the same time fitting the γ -ray data, rather than fitting the data using rigorous statistical techniques.

7. A Detailed Case Study: Terzan 5

7.1 Leptonic Modelling of the Broadband SED

Following the idea of Kopp et al. [17], we propose the X-ray data points to a new component that has not been considered before - one due to pulsed, magnetospheric SR (a HESR component).

Table 1: Sample parameter combinations that lead to a balance of the X-ray-implied energetics for Terzan 5. Columns refer to conversion efficiency η of spin-down to particle luminosity, the average spin-down \dot{E} and number of pulsars N for both detected / visible (vis) and undetected / invisible (invis) X-ray emitting MSPs; also included are the minimum and maximum spin-down luminosities of the MSP population as well as the luminosity function slope γ_L .

η_X	\dot{E}_{invis}	\dot{E}_{vis}	\dot{E}_{min}	\dot{E}_{max}	γ_L	N_{vis}^X	N_{invis}^X	N_{tot}^X
0.05%	3.0×10^{33}	9.2×10^{34}	10^{31}	2.4×10^{35}	-0.19	43	45	88
0.05%	3.5×10^{32}	1.8×10^{35}	10^{29}	10^{36}	0.21	22	399	421
0.5%	1.2×10^{32}	3.8×10^{34}	10^{31}	10^{36}	0.50	10	116	126
0.5%	1.5×10^{32}	2.8×10^{34}	10^{31}	3.6×10^{35}	0.40	14	96	110
1%	7.4×10^{31}	2.5×10^{34}	10^{31}	2.0×10^{36}	0.60	8	95	103
1%	1.3×10^{32}	2.4×10^{34}	3.0×10^{31}	2.9×10^{36}	0.64	8	53	61
1%	2.5×10^{32}	2.0×10^{34}	10^{32}	3.0×10^{36}	0.69	10	27	37

This is in addition to the LESR component. In order to be consistent in terms of the pair multiplicity inferred by the LESR and HESR components, we invoke an inner region of the polar cap where the M_{inv} is low, and use a high M_{vis} in the slot gap (connected to the HESR component); yet, the total multiplicity of particles coming from the whole polar cap M_{avg} , which is the weighted average of M_{inv} and M_{vis} , is equal to the value implied by fitting the unpulsed LESR to the data. Our predicted SED (Figure 4) shows the GC model output in blue and the pulsar model predictions in red. The pair synchrotron emission (HESR component) matches the observed X-ray spectrum quite well.

7.2 Balancing the Energetics of the Embedded MSP Population

Although our joint model provides reasonable fits to the *Fermi* and *Chandra* data, we still have to consider whether this MSP scenario is plausible in terms of the sensitivity of *Chandra* and energetics. We modelled the pulsar population via a parametric spin-down luminosity function $dN/d\dot{E} = N'_0(\dot{E}/\dot{E}_0)^{-(\gamma_L+1)}$, with N'_0 a normalisation constant and found different solutions that lead to a balance of energetics. Table 1 shows a number of parameter combinations that satisfy the observational constraints. Different choices of $\langle \dot{E}_{\text{vis}} \rangle$ will favour a different solution.

8. Estimating Uncertainties in the Predicted VHE Flux of GCs

We assessed uncertainties in the predicted VHE flux of GCs for our leptonic model, modelling the IC γ -ray flux expected from several GCs to see whether the predicted flux exceeds the CTA sensitivity and whether we can satisfy the H.E.S.S. upper limits with a range of predicted fluxes.

8.1 Integral Flux Upper Limits: the H.E.S.S. GC Population

We used a Monte-Carlo method to calculate the single-GC and stacked integral VHE flux of 15 GCs with uncertainties due to the uncertainty in model parameter. We did this by randomising over seven free parameters: Cluster field B , injection spectral slope Γ , number of stars N_* , distance d , conversion efficiency η , average spin-down power \dot{E} , and number of MSPs N_{MSP} ; we also assumed Bohm diffusion.

In Figure 5 we show how the distribution of \log_{10} of the integral flux becomes smooth as we increase the resolution of the grid over which free parameters are sampled. We also randomly sample integral fluxes for a different total number of trials N_t (see Figure 6) from the grid to show

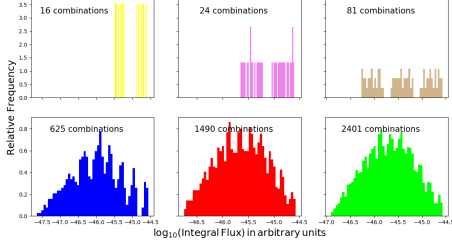


Figure 5: Histograms of $\log_{10}(F(E > 0.72 \text{ TeV}))$ in arbitrary units, indicating how we build up statistics for the flux distribution for a finer grid in parameter space.

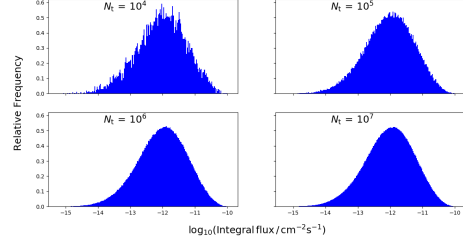


Figure 6: Histograms of $\log_{10}(F(E > 0.72 \text{ TeV}) / \text{cm}^{-2}\text{s}^{-1})$ for different N_t for 47 Tucanae, and for 7 free parameters.

convergence as the number of trials converge to the number of combinations: $N_t \rightarrow N_{\text{comb}}$. We note that undersampling will not give a smooth flux distribution, while oversampling will lead to convergence.

In Figure 7 we show the distribution of the \log_{10} of livetime-weighted flux for all selected H.E.S.S. GCs. The green histogram shows the first set of parameter combinations (i.e., $d' \in [\frac{d}{2}, \frac{d}{\sqrt{2}}, d, \sqrt{2}d, 2d]$, $N'_* \in [\frac{N}{2}, \frac{N_*}{\sqrt{2}}, N_*, \sqrt{2}N_*, 2N_*]$, $B \in [1, 9]$ in steps of $2\mu\text{G}$, $\Gamma \in [1.7, 2.9]$ in steps of 0.3, $\eta \in [0.005, 0.08]$ in steps of 0.0075, $\log_{10}\langle\dot{E}\rangle \in [33.7, 34.7]$ in steps of 0.1, and $N_{\text{MSP}} \in [5, 150]$ in steps of 10.) with the median stacked flux exceeding the upper limit by a factor of 7.6. We therefore considered a second parameter set: $\eta \in [0.003, 0.03]$ in steps of 0.003, $\log_{10}\langle\dot{E}\rangle \in [33, 34]$ in steps of 0.1, and $N_{\text{MSP}} \in [5, 50]$ in steps of 5, associated with the blue histogram. This choice of parameters may seem a bit arbitrary, but given the freedom in model parameters, there is no unique way of reducing the GC flux.

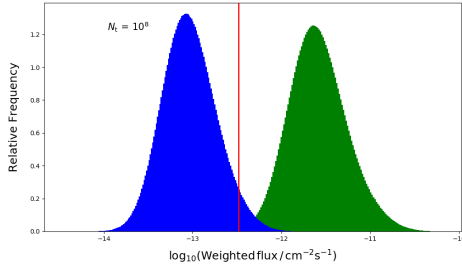


Figure 7: Distribution of $\log_{10}(F_w(E > E_{\text{th}}) / \text{cm}^{-2}\text{s}^{-1})$ for all GCs. The green histogram is associated with the first parameter combination, while the blue one is for the second parameter combination. The red line represents the stacked upper limit.

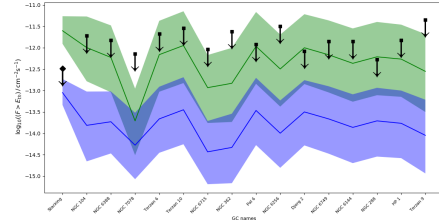


Figure 8: Flux upper limits (black diamond and squares with arrows) on the observed γ -ray flux from the population of GCs, as well as the predicted flux medians plus 1σ uncertainties (green and blue bands for each of the two parameter combinations). The first entry indicates the stacked (live-time-weighted) flux with 1σ uncertainties.

Finally, we graphically summarise the fluxes we obtained for both the stacked as well as single-GC cases in Figure 8. The black diamond and squares and arrows correspond to the observational upper limits, while the green and blue squares and error bars are for the median fluxes and 1σ uncertainty intervals, for the two different parameter combinations as discussed above. There are indeed parameter combinations that yield fluxes below all of these observational upper limits. One example is provided by combinations of degenerate parameters yielding a lower Q_0 ; there may also be other parameter combinations that can lower the flux. Further constraints derived from future

observations may aid in breaking such degeneracies.

8.2 Differential Flux Predictions: M15 and ω Cen

MAGIC has recently published differential flux upper limits for M15 [16]. We created a distribution of differential fluxes of the northern GC M15 and calculate the median and 1σ uncertainties of the \log_{10} of fluxes by finding the 16th, 50th and 84th percentiles.

Figure 9 shows the upper limits from 165 hours of MAGIC observations on the differential flux, the predicted spectrum for a few different combinations of model parameters and the median values (dashed green line) with 1σ errors (light green band). We note that the differential data are much more constraining than the integral data since there are 13 points of comparison instead of 1. We satisfy the MAGIC flux upper limits for our choice of parameters. We used the same

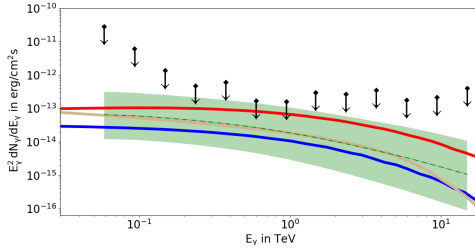


Figure 9: Differential flux upper limits (black diamonds with arrows) on the γ -ray flux from M15 plus a few typical model spectra (solid lines) for typical parameter combinations, as well as predicted medians and 1σ error bars (green error band).

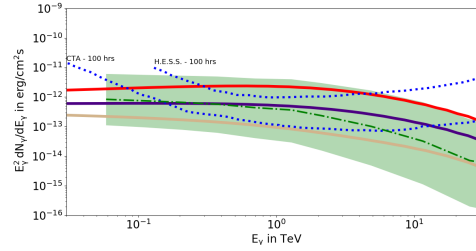


Figure 10: Differential flux predictions (green error band) for ω Cen, the solid lines indicating example predictions. The blue dashed lines represent the H.E.S.S. and CTA sensitivity curves for 100 hours of observations.

method on the southern GC ω Cen, which has recently been confirmed to harbour five radio MSPs by the Parkes Radio Telescope [29]. We compare its predicted differential fluxes with the H.E.S.S. and CTA sensitivity curves for 100 hours of observation. We also indicate typical predicted γ -ray spectra for a few choice of parameter combinations (see Figure 10).

9. Conclusions

We used a leptonic emission code to make flux predictions for GCs and performed a parameter study, varying six model parameters. We found that the parameters of the individual GCs were uncertain and quite unconstrained by the available data. We found that H.E.S.S. may detect two more GCs, i.e. 47 Tucanae and NGC 6388, if the clusters are observed for 100 h. The five most promising GCs for future TeV observations are NGC 6388, 47 Tucanae, Terzan 5, Djorg 2, and Terzan 10. Future multi-wavelength studies should allow us to constrain some parameters better as well as discriminate between competing radiation models. We obtained new *Fermi* data that we could fit using a model for the cumulative CR from a population of MSPs embedded within Terzan 5. These data proved to be constraining for the low-energy tail of the unpulsed IC component, as well as for the number of MSPs emitting CR. We showed that we could fit the radio spectral points by invoking an LESR component that might extend into the optical range. We invoked a new spectral component to explain the hard *Chandra* spectrum: cumulative SR from pair plasma in MSP magnetospheres. We argued that the required energetics and numbers of the MSP source

population needed to reproduce the detected diffuse X-ray emission are plausible, even though they are not very well constrained. We also assessed uncertainties in the predicted VHE γ -ray flux of GCs for a given leptonic model due to uncertainties in model parameters, and gave theoretical guidance to CTA's observational strategy. We found that the total integral weighted flux violated the H.E.S.S. upper limits for our first combination of parameters, but the second parameter combination satisfied the stacking upper limits. We lastly performed a case study on two GCs, M15 and ω Cen to assess their predicted fluxes plus errors, and found that the differential upper limits were more constraining for M15 than the H.E.S.S. integral flux upper limits. We calculated the TeV flux for ω Cen and showed that this GC may be a possible candidate to be observed by H.E.S.S. or CTA. One can improve the precision of predictions of GC fluxes by increasing measurement accuracy on model parameters. Models should thus undergo scrutiny by also taking into account the effect of parameter uncertainty on their predictions as they are confronted with new data.

Acknowledgments

We acknowledge discussions with James Allison and Leonard Santana. This work is based on the research supported wholly / in part by the National Research Foundation of South Africa (NRF; Grant Numbers 87613, 90822, 92860, 93278, and 99072). The Grantholder acknowledges that opinions, findings and conclusions or recommendations expressed in any publication generated by the NRF supported research is that of the author(s), and that the NRF accepts no liability whatsoever in this regard. The Virtual Institute for Scientific Computing and Artificial Intelligence (VI-SCAI) is gratefully acknowledged for operating the High Performance Computing (HPC) cluster at the University of Namibia (UNAM). VI-SCAI is partly funded through a UNAM internal research grant. This study was financially supported by the African German Network of Excellence in Science (AGNES), through the "Programme Advocating Women in Science, Technology, Engineering and Mathematics".

References

- [1] L.M. Krauss and B. Chaboyer, *Age Estimates of Globular Clusters in the Milky Way: Constraints on Cosmology*, *Science* **299** (2003) 65.
- [2] W.E. Harris, *A New Catalog of Globular Clusters in the Milky Way*, *arXiv:1012.3224* (2010) .
- [3] E. Dalessandro and Cosmic-Lab Team, *Blue straggler stars in globular clusters: observational results*, *MmSAI* **87** (2016) 493.
- [4] P.C.C. Freire, A. Ridolfi, M. Kramer, C. Jordan, R.N. Manchester, P. Torne et al., *Long-term observations of the pulsars in 47 Tucanae - II. Proper motions, accelerations and jerks*, *MNRAS* **471** (2017) 857 [1706.04908].
- [5] A.-C. Clapson, W. Domainko, M. Jamrozy, M. Dyrda and P. Eger, *Multi-wavelength environment of the Galactic globular cluster Terzan 5*, *A&A* **532** (2011) A47.
- [6] P. Eger, W. Domainko and A.-C. Clapson, *Chandra detection of diffuse X-ray emission from the globular cluster Terzan 5*, *A&A* **513** (2010) A66 [1002.0711].

- [7] P. Eger and W. Domainko, *A search for diffuse X-ray emission from GeV-detected Galactic globular clusters*, *A&A* **540** (2012) A17.
- [8] E.M.H. Wu et al., *Chandra Detection of a New Diffuse X-Ray Component from the Globular Cluster 47 Tucanae*, *ApJL* **788** (2014) L40.
- [9] C.O. Heinke, R. Wijnands, H.N. Cohn, P.M. Lugger, J.E. Grindlay, D. Pooley et al., *Faint X-Ray Sources in the Globular Cluster Terzan 5*, *ApJ* **651** (2006) 1098 [[astro-ph/0606253](#)].
- [10] L.E. Rivera-Sandoval et al., *Discovery of near-ultraviolet counterparts to millisecond pulsars in the globular cluster 47 Tucanae*, *MNRAS* **453** (2015) 2707 [[1508.05291](#)].
- [11] C. Pallanca et al., *Optical companions to millisecond pulsars in globular clusters.*, *MemSAI* **87** (2016) 526.
- [12] S. Abdollahi et al., *Fermi Large Area Telescope Fourth Source Catalog*, *ApJS* **247** (2020) 33 [[1902.10045](#)].
- [13] A. Abramowski et al., *Very-high-energy gamma-ray emission from the direction of the Galactic globular cluster Terzan 5*, *A&A* **531** (2011) L18.
- [14] H. Anderhub et al., *MAGIC upper limits to the VHE gamma-ray flux of 3C 454.3 in high emission state*, *A&A* **498** (2009) 83.
- [15] F. Aharonian et al., *HESS upper limit on the very high energy γ -ray emission from the globular cluster 47 Tucanae*, *A&A* **499** (2009) 273 [[0904.0361](#)].
- [16] V.A. Acciari et al., *Deep observations of the globular cluster M15 with the MAGIC telescopes*, *MNRAS* **484** (2019) 2876 [[1901.04367](#)].
- [17] A. Kopp, C. Venter, I. Büsching and O.C. De Jager, *Multi-wavelength Modeling of Globular Clusters - The Millisecond Pulsar Scenario*, *ApJ* **779** (2013) 126.
- [18] H. Ndiyavala, *Search for best globular cluster candidates for H.E.S.S. and CTA*, *Unpublished dissertation, North-West University, Potchefstroom, South Africa*, 2016.
- [19] H. Ndiyavala, C. Venter and P. Paulus Kruger, *Investigating gamma-ray fluxes from globular clusters*, *arXiv e-prints* (2017) arXiv:1712.07872 [[1712.07872](#)].
- [20] H. Ndiyavala, P.P. Krüger and C. Venter, *Identifying the brightest Galactic globular clusters for future observations by H.E.S.S. and CTA*, *MNRAS* **473** (2018) 897 [[1708.09817](#)].
- [21] H. Ndiyavala, C. Venter, T.J. Johnson, A.K. Harding, D.A. Smith, P. Eger et al., *Probing the Pulsar Population of Terzan 5 via Spectral Modeling*, *ApJ* **880** (2019) 53 [[1905.10229](#)].
- [22] H. Ndiyavala-Davids, C. Venter, A. Kopp and M. Backes, *Assessing uncertainties in the predicted very high energy flux of globular clusters in the Cherenkov Telescope Array era*, *MNRAS* **500** (2021) 4827 [[2011.07486](#)].

- [23] E.N. Parker, *The passage of energetic charged particles through interplanetary space*, *P&SS* **13** (1965) 9.
- [24] P. Prinsloo, C. Venter, I. Büsching and A. Kopp, *Modelling the stellar soft-photon energy density profile of globular clusters*, in *Proc. SAIP 2013* (2013) [1311.3791].
- [25] I.V. Moskalenko and A.W. Strong, *Production and Propagation of Cosmic-Ray Positrons and Electrons*, *ApJ* **493** (1998) 694 [astro-ph/9710124].
- [26] A.K. Harding and C. Kalapotharakos, *Synchrotron Self-Compton Emission from the Crab and Other Pulsars*, *ApJ* **811** (2015) 63 [1508.06251].
- [27] M. Cadelano, S.M. Ransom, P.C.C. Freire, F.R. Ferraro, J.W.T. Hessels, B. Lanzoni et al., *Discovery of Three New Millisecond Pulsars in Terzan 5*, *ApJ* **855** (2018) 125 [1801.09929].
- [28] A.A. Abdo et al., *A population of gamma-ray emitting globular clusters seen with the Fermi Large Area Telescope*, *A&A* **524** (2010) A75.
- [29] S. Dai, S. Johnston, M. Kerr, F. Camilo, A. Cameron, L. Toomey et al., *Discovery of Millisecond Pulsars in the Globular Cluster Omega Centauri*, *ApJ* **888** (2020) L18 [1912.08079].